Linewidth-narrowing phenomena with intersubband cavity polaritons

Francis J. Murphy,[1,*] Alexey O. Bak,[1] Mary Matthews,[2] Emmanuel Dupont,[3] Hemmel Amrania,[1] and Chris C. Phillips[1]

[1]*Experimental Solid State Physics, Blackett Laboratory, Imperial College, London SW7 2AZ, United Kingdom*

[2]*GAP-Biophotonics, Université de Genève, Chemin de Pinchat 22, 1211 Geneva 4, Switzerland*

[3]*National Research Council, Ottawa, Ontario K1A 0R6, Canada*

Absorption spectra of strongly coupled intersubband cavity polaritons have been measured, using a tunable midinfrared quantum cascade laser, with high angular and spectral resolution. Pronounced linewidth narrowing of the polaritons around the anticrossing was found, with polariton linewidths narrower (4.2 meV) than both the bare intersubband transition linewidth and empty cavity linewidth (6.2 and 6 meV, respectively), at room temperature. This is due to variations in the degree of spatial averaging of the in-plane quantum-well disorder as the polariton's extended coherence length is increased by the photonic coupling over the value corresponding to the bare intersubband transition coherence length.

PACS number(s): 73.21.Fg, 71.36.+c, 78.67.De

I. INTRODUCTION

The coupling between intersubband transitions (ISBTs) in quantum wells (QWs), and confined photons in a microcavity, leads to the formation of quasiparticles known as intersubband cavity polaritons (ICPs). When in the strong coupling regime, the ISBT and the microcavity modes anticross and two ICP peaks become resolvable in the absorption spectra, their minimum energy separation being characterized by the vacuum-Rabi energy. These separate branches are known as the upper and lower polariton branches (UPB and LPB).

Since their first observation in 2003 [1,2], ICPs have been studied extensively in terms of their dispersion properties [3], electron dynamics [4,5], ultrafast light-matter phenomena [6], quantum field characteristics [7], and for the generation of entangled photons [8]. Furthermore, ICPs offer the possibility of creating terahertz light emitters, presenting an alternative to laser-based terahertz sources which face fundamental limits at room temperature [9–11].

Here, we present quantum cascade laser (QCL)-based absorption spectra of ICPs. Compared with previous studies that typically used thermal sources and wide-aperture optics, this laser-based spectroscopy gives superior angular resolution, which translates into a much higher energy resolution for measuring the ICP linewidths [12]. The focus of this paper is on the measurement of the linewidths of the ICPs, through angle-resolved reflection-absorption laser spectroscopy in the midinfrared (112–241 meV, $\sim$900–1940 cm^{-1}, $\lambda \sim$ 11–5 μm). Significantly, we have observed linewidth-narrowing effects, where the UPB and LPB show sharp linewidths that can only be understood if the scattering rates of the matter part of the polariton are reduced below their bare ISBT and empty microcavity values.

Models of the sample give an effective ISBT linewidth of $\delta_{\mathrm{ISBT}}|_{\mathrm{anticrossing}} \approx 4$ meV at the anticrossing point. This effect is interpreted as a disorder averaging phenomenon in which the large spatial extent of the ICP compared to that of the bare ISBT electron effectively averages the disorder in the QW width, thereby narrowing the ICP.

II. MICROCAVITY SAMPLE

The sample studied is a multiquantum well (MQW) slab within a waveguide microcavity (Fig. 1). It was grown on a 500-μm-thick semi-insulating GaAs substrate and comprised a 0.8-μm-thick n-GaAs mirror layer doped at $N_D = 2 \times 10^{18}$ cm^{-3}; a 140 repeat MQW; followed by a back mirror comprising a 0.394-μm-thick n-GaAs layer, with the same doping as the coupling mirror. The sample was capped, top and bottom, with a 200 nm/9 nm Au/Ti layer. Each QW period comprised a 6-nm GaAs well of equivalent two-dimensional (2D) electron density $n_s = 2 \times 10^{10}$ cm^{-2}, and a 29-nm Al$_{0.24}$Ga$_{0.76}$As barrier, with the central 20-nm Si doped at a concentration of 10^{16} cm^{-3}. The MQW slab was 4.9 μm thick in total.

At the wavelengths of interest, the n-doped 0.8- and 0.394-μm GaAs mirror layers had a negative permittivity and behaved as metallic mirrors, forming the microcavity. The QCL light was coupled into the sample through the polished edge of the 500-μm semi-insulating GaAs substrate and was then coupled in and out of the microcavity itself via frustrated total internal reflection, before undergoing a reflection from the lower Au cap and leaving the substrate (see Fig. 1). The sample was polished into a lozenge, with facets at an angle $\sim$10° to the z axis, so that the anticrossing point could be scanned through with the QCL beam incident at external incidence angles that were close to the facet normal.

The bare ISBT is a bound to quasibound transition of energy $\hbar\omega_{\mathrm{ISBT}} = 129.1$ meV and linewidth $\delta_{\mathrm{ISBT}} = 6.2$ meV at room temperature. These values were obtained by measuring the UPB spectrum at incident angles ($\varphi \approx 62.0°$) that were so far away from the anticrossing point that the UPB's photonic component is negligible, and the UPB lineshape takes its properties entirely from the ISBT. The anticrossing spectrum occurs at $\varphi \approx 72.3°$ and shows an ICP separation minimum of 13.6 meV, i.e. a polariton splitting energy some 10% of the ISBT energy.

III. EXPERIMENTAL SETUP

The spectroscopy was performed at room temperature using commercial QCLs (MIRcat from Daylight Solutions

---
*Corresponding author: fjm06@ic.ac.uk
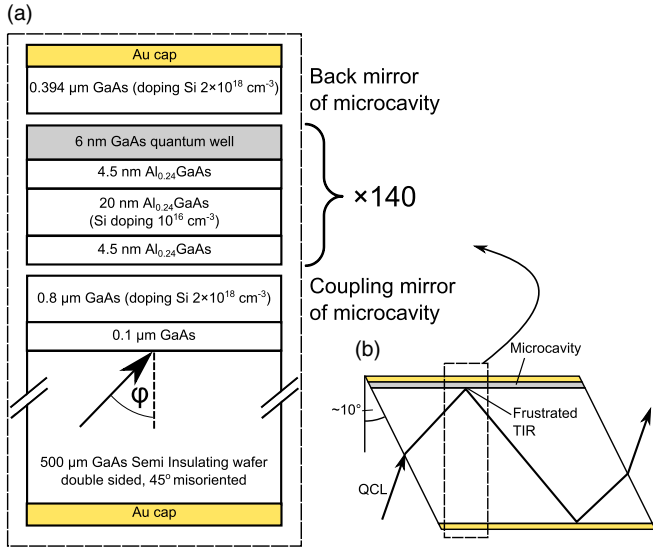
FIG. 1. (Color online) (a) Structure of sample and definition of incident coupling angle φ. The back and coupling mirror of the microcavity are n-doped layers of GaAs. The ISBT within the QWs is a bound-to-quasibound transition at 129.1 meV. (b) Geometry for coupling into the microcavity. Quantum cascade laser light is coupled in and out of the sample via the facet of the 500-μm SI-GaAs substrate; the light then couples into and out of the microcavity via frustrated total internal reflection, before reflecting from the lower Au cap and exiting the sample. The sample facet is polished at $\sim 10°$ to perpendicular so that the incoming beam enters the semiconductor close to the facet normal at the internal propagation angle corresponding to the anticrossing point.

and LaserTune from Block Engineering), tunable from $\sim$112–241 meV (900–1940 cm^{-1}, $\lambda \sim$ 11–5 μm) with resolution of $\sim$0.12 meV ($<$1 cm^{-1}) and pulsed at 100 kHz with 100 kWcm^{-2} of CW intensity.

The sample was mounted on a rotating stage, and at each incident angle φ, the laser was step scanned through the midinfrared photon energy range. The QCL beam was linearly polarized such that it had transverse magnetic (TM) and transverse electric (TE) components with respect to the plane of incidence on the microcavity. The TM-polarized ISBT absorption selection rule means that the TE-polarized light does not interact with ISBTs and could be used to give background spectra for ratiometric calibration. Absorption is given by $-\ln(I_{\text{TM}}/I_{\text{TE}})$, where I_{TM} and I_{TE} are the TM- and TE-polarized intensities transmitted through the sample. The QCL beam divergence gave an angular resolution of $\Delta\varphi \sim 0.3°$ within the substrate, which compares with the $\Delta\varphi \sim 1.5°$ achievable with typical high numerical aperture thermal sources. The resultant energy resolution depends on the angular resolution and on the slope of the ICP dispersion curve. The linewidths quoted are the full width at half maxima (FWHM) of the ICP absorption peaks.

IV. LINEWIDTH RESULTS

A. Narrow polariton linewidths at anticrossing

Figure 2 shows the measured absorption spectra at incident angles spanning the anticrossing point, and Fig. 3 shows the
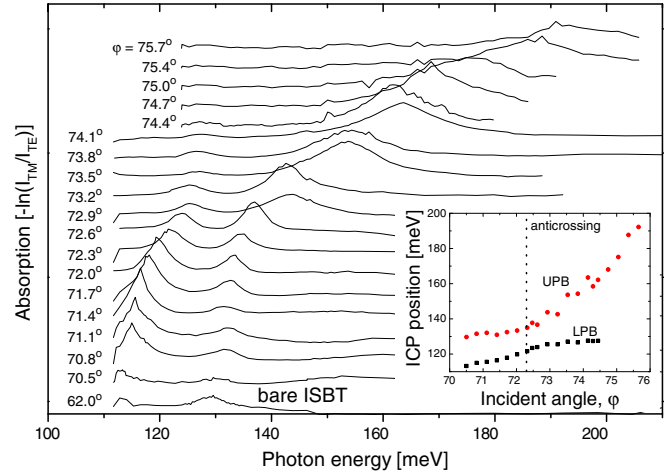
FIG. 2. (Color online) Absorption spectra with offset showing twin peaks of the ICPs across a range of coupling angles, with anticrossing around $\varphi = 72.3°$. Also shown is the electroniclike polariton at $\varphi = 62.0°$, which may be used for the bare ISBT absorption properties. Inset is the dispersion curve of the ICPs showing the anticrossing.

measured linewidths. Figure 4 compares the measured spectra with the output of the electromagnetic modeling discussed in detail in Sec. V B. There was no laser intensity dependence to the properties of the ICPs in the experimental intensity range.

As a starting point, the linewidths of ICPs may be understood, using a linear dispersion theory approach, as a
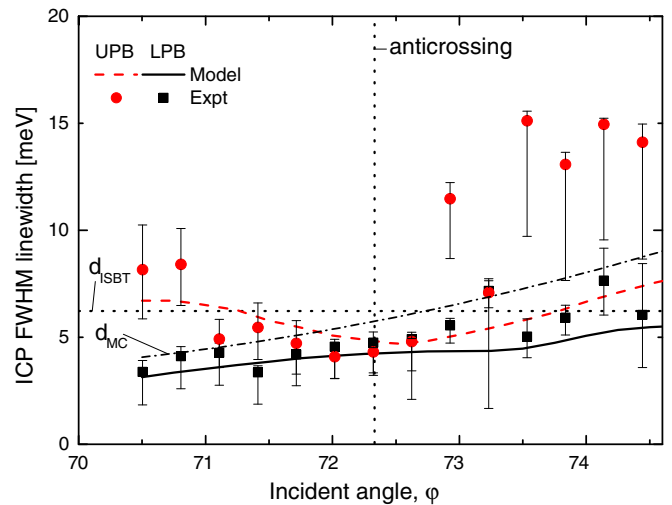
FIG. 3. (Color online) Full width at half maximum linewidth data of UPB (LPB), $\delta_{\text{UPB(LPB)}}$ red circles (black squares). The vertical dotted line corresponds to anticrossing point. Full width at half maximum from model (Sec. V B) are shown for the UPB/LPB by a dashed red/solid black line. The measured bare ISBT linewidth δ_{ISBT} is indicated (horizontal dotted line), as is the modeled microcavity linewidth δ_{MC} (dash-dotted line). The data and model both give regions of $\delta_{\text{UPB}}, \delta_{\text{LPB}} < \delta_{\text{ISBT}}, \delta_{\text{MC}}$ around the anticrossing point. Error bars include the lower bound of linewidths in the case of perfect resolution and are larger where the dispersion curves (Fig. 2) are steeper.
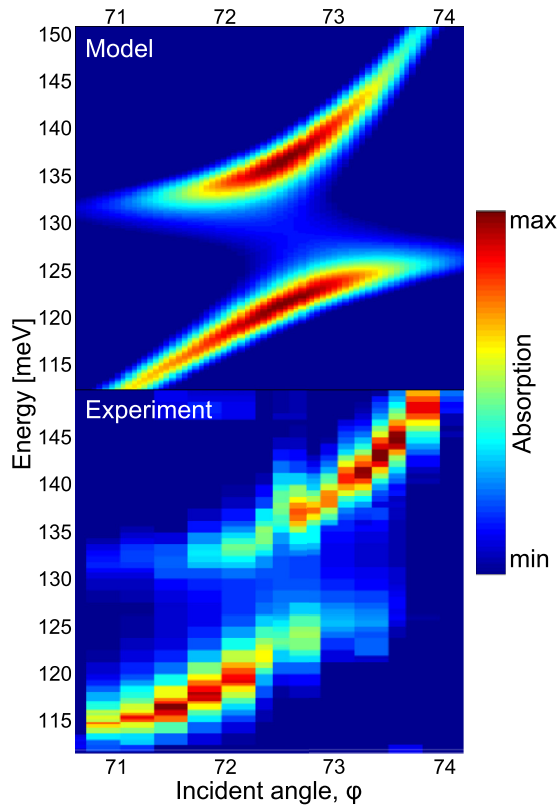
FIG. 4. (Color online) (Upper) Absorption spectra for the sample, modeled with an effective medium approach and transfer matrix formalism. The assumed parameters are detailed in Sec. V. (Lower) Colormap of measured absorption spectra from Fig. 2 showing good agreement with model.

weighted average of the constituent ISBT and microcavity Lorentzian linewidths. At the anticrossing, this is an arithmetic average

$$\delta_{ICP} = \tfrac{1}{2}(\delta_{ISBT} + \delta_{MC}). \qquad (1)$$

The observed ICP linewidths are immediately at odds with this simple picture because they exhibit *subaverage* linewidths, i.e. $\delta_{UPB}, \delta_{LPB} < \tfrac{1}{2}(\delta_{ISBT} + \delta_{MC})$, e.g. $\delta_{UPB} = 4.3$ meV and $\delta_{ISBT} = 6.2$ meV, $\delta_{MC} \approx 6$ meV at $\varphi = 72.3°$ (i.e. the anticrossing point). See Fig. 3.

To understand this, we must first calculate the linewidth of the pure optical cavity mode, i.e. the microcavity resonance linewidth when it is devoid of ISBTs δ_{MC}. To this end, we modeled (Sec. V) the full as-grown sample structure, but with the electron doping set to zero, to extract the linewidths of the fundamental TM mode. Because of the angular variations in the way light is reflected at the various boundaries in the sample, the calculated microcavity linewidths themselves vary with angle, from $\delta_{MC} \approx 4$ to 10 meV, with a value of 6 meV at the anticrossing. The result was that, given a bare ISBT linewidth of $\delta_{ISBT} = 6.2$ meV, the observation of the sharp ICP linewidths (down to $\delta_{UPB} = 4.3$ meV at the anticrossing point) could only be explained if the bare ISBT linewidth was itself narrowing as the system was tuned through the anticrossing point.

B. Two models to consider

To extract the variable behavior of the ISBT linewidth δ_{ISBT}, the ICP system was modeled assuming two possible extensions of the standard linear dispersion approach. The first assumed that the ISBT was homogenously broadened, dominantly by interface roughness scattering, but that disorder averaging effects took place that resulted in a Lorentzian lineshape whose width δ_{ISBT} varied as the system was tuned through the anticrossing point. The second assumed that the QW disorder was such that the ISBT linewidth had a significant inhomogenous component (contributing a Gaussian component to the lineshape) giving a so-called "Voigt" lineshape, as has been previously employed to model narrowing of exciton cavity polaritons [13,14].

V. COMPUTATIONAL MODELS

A. Homogenously broadened "Variable Lorentzian" model

The periodicity of the MQW is much less than the wavelength of light, so the overall MQW layer can be described to a good approximation as an effective anisotropic dielectric medium. Here, we model its dielectric response with the method described in Ref. [15], but we treat the Lorentzian FWHM as a fitting variable that depends on the angle of incidence [16], i.e. $\delta_{ISBT} = \delta_{ISBT}(\varphi)$. We then use a transfer matrix formalism [17] to propagate a plane wave through the microcavity sample to give the modeled spectra of Fig. 4.

The following parameters were used to model the MQW structure: background dielectric constants of $\varepsilon_{GaAs} = 10.89$ and $\varepsilon_{AlGaAs} = 10.21$; an effective mass $m^* = 0.063$ for the electrons in the well; and a calculated ISBT energy of $\hbar\omega_{ISBT} = 129$ meV for a 6-nm QW width. The n-doped GaAs microcavity mirrors were modeled using a Drude dielectric response, with an electron scattering time of $\tau = 1$ ps (determined by LO phonon scattering [18]) and a doping concentration of 2.6×10^{18} cm^{-3}. The values used for the remaining parameters were as described in Sec. II.

This approach leads to an extracted Lorentzian linewidth $\delta_{ISBT}(\varphi)$ which, at 6.2 meV, is broadest away from the anticrossing point, and goes through a minimum $\delta_{ISBT}|_{anticrossing} \approx 4$ meV at the anticrossing point.

Previous studies [19] have found that, for symmetrical QWs at these temperatures and doping levels, where the effects of conduction band nonparabolicity on the ISBT lineshape can be neglected, the combined effects of phonon (acoustic and optical), impurity and alloy disorder scattering combined contribute ~ 1 meV to the bare ISBT linewidth. The dominant contribution comes from interface roughness scattering (IRS).

If the fluctuation $\Delta(\mathbf{r})$ in the QW width as a function of $\mathbf{r} = (x, y)$ in the well plane has a correlation function

$$\langle \Delta(\mathbf{r})\Delta(\mathbf{r}')\rangle = \Delta^2 \exp\left(-\frac{|\mathbf{r} - \mathbf{r}'|^2}{\Lambda^2}\right), \qquad (2)$$

where Δ is the root mean squared height of the roughness fluctuations, and Λ (typically 0.3–0.7 nm) [19] their in-plane correlation length, then the dominant IRS scattering channel is an intrasubband process, which is unscreened and driven by a scattering potential, proportional to the rate of change of ISBT energy $\hbar\omega_{ISBT}$ with well width d_w. This gives an overall

scattering rate

$$\delta_{\text{intra}}^{(\text{IRS})} = \frac{m_{\text{scat}}\Delta^2\Lambda^2}{\hbar^2}\left[\frac{\partial(\hbar\omega_{\text{ISBT}})}{\partial d_W}\right]^2\int_0^\pi d\theta \exp\left(\frac{-q^2\Lambda^2}{4}\right),$$
$$\text{(3)}$$

where m_{scat} is the effective mass of the scattered electron, q is the scattering wavevector, related to the electron wavevector k by

$$q^2 = 2k^2(1 - \cos\theta). \tag{4}$$

For electron wavelengths that are sufficiently longer than Λ, this rate scales simply as $\sim m_{\text{scat}}\Lambda^2\Delta^2$, thus we see that, as the bare ISBT mixes with the photon in the strong coupling regime, the combined effect of lowering the in-plane effective mass, and the effective reducing of the value of Δ^2 as the polariton wavefunction progressively averages over larger in-plane QW areas, will reduce the IRS contribution to the bare ISBT linewidth and thus explain the subaveraging effect seen in Fig. 3.

B. Lorentzian-Gaussian convolution model

The second model kept all the same properties as in Sec. V A. but allows for the fact that the fluctuations in QW width might also be happening on a sufficiently coarse length scale, either between wells or between spatially separated regions of the same well, to give a significant inhomogeneously broadened component to the ISBT linewidth [20]. In this case, the lineshape is best described as a convolution of Lorentzian and Gaussian lineshapes, the Voigt profile, or plasma dispersion function. Accordingly, the MQW was modeled as in Ref. [15], but with the perpendicular dielectric response of the effective medium altered to reflect the Voigt profile as

$$\frac{1}{\varepsilon_\perp(\omega)} = \frac{1}{\epsilon_\perp} - \frac{e^2 n_s f_{12}\hbar\pi}{2m^*\varepsilon_0\varepsilon_w^2\omega}\left\{\frac{i\text{Re}[w(z)] + \text{Im}[w(z)]}{\sigma\sqrt{2\pi}}\right\}, \quad \text{(5)}$$

where $\frac{1}{\epsilon_\perp} = \frac{d_w}{d_p}\frac{1}{\varepsilon_w} + \frac{d_b}{d_p}\frac{1}{\varepsilon_b}$, d_w and d_b are the well and barrier widths, d_p is the periodicity, ε_w and ε_b are the well and barrier background dielectric constants, n_s is the 2D electron density, f_{12} the oscillator strength of an ISBT, e (m^*) the electron charge (effective mass), and σ the Gaussian parameter related to the Gaussian FWHM $\xi = 2\sigma\sqrt{2\ln 2}$. Here, $w(z) = e^{-z^2}\text{erfc}(-iz)$ is the Fadeeva function, closely related to the Voigt profile, where $\text{Re}[w(z)]/\sigma\sqrt{2\pi}$ is the Voigt profile, and [21]

$$z = [\hbar(\omega_{\text{ISBT}} - \omega) + i\gamma/2]/\sigma\sqrt{2}. \tag{6}$$

The model is shown in Fig. 4. Fitting this model to the data gave a Lorentzian contribution of $\gamma \approx 4$ meV to the ISBT

linewidth and Gaussian contribution of $\xi \approx 3.6$ meV of the total $\delta_{\text{ISBT}} = 6.2$ meV. The extracted linewidths are shown in Fig. 3 giving good agreement with the data. There is a discrepancy between the data and model for the UPB at higher angles, attributed to the reduction in energy resolution due to the steeper dispersion curve in this region.

In the same way as with the homogenously broadened IRS scattering mechanism, in this inhomogenously broadened scenario, the increased coherence length of the ICP as the bare ISBT mixes with the cavity photon is capable of averaging over a greater region of QW disorder, thereby reducing the ISBT broadening. The inhomogeneous component of the bare ISBT is effectively forgotten, leaving just the homogeneous linewidth to contribute to the linewidth at the anticrossing: $\delta_{\text{ISBT}}|_{\text{anticrossing}} \approx \gamma \approx 4$ meV.

VI. CONCLUSION

In the absence of definitive knowledge of the QW disorder statistics, it is likely that the real physical behavior of the system is a mix of these two discussed models. However, they both share the novel feature that the unique nature of the ISBT scattering mechanisms means that the physics of strongly coupled systems like this cannot be understood within a linear dispersion model, and a more detailed microscopic analysis of the scattering is required.

In conclusion, we have presented high-resolution angle-resolved spectra of intersubband cavity polaritons that demonstrate pronounced linewidth narrowing effects at angles around the anticrossing. The measurements benefit from using a tunable laser source (QCL) with high angular resolution, compared to traditional thermal source. Because of the angular dispersion in the system, this high angular resolution is needed to achieve high energy resolution, and it has allowed us to measure the true linewidths of ICPs.

We find ICP linewidths that become subaverage, i.e. narrower than the average of the bare ISBT and microcavity linewidths $\delta_{\text{ICP}} < \frac{1}{2}(\delta_{\text{ISBT}} + \delta_{\text{MC}})$. This is thought to be due to the increase in coherence length of the ICP compared to the ISBT, allowing the quasiparticle to better average over the spatial disorder in the QWs.

---

[1] D. Dini, R. Köhler, A. Tredicucci, G. Biasiol, and L. Sorba, Phys. Rev. Lett. **90**, 116401 (2003).

[2] E. Dupont, H. C. Liu, A. J. SpringThorpe, W. Lai, and M. Extavour, Phys. Rev. B **68**, 245320 (2003).

[3] M. Załużny and W. Zietkowski, Phys. Rev. B **88**, 195408 (2013).

[4] L. Sapienza, A. Vasanelli, R. Colombelli, C. Ciuti, Y. Chassagneux, C. Manquest, U. Gennser, and C. Sirtori, Phys. Rev. Lett. **100**, 136806 (2008).

[5] A. A. Anappara, A. Tredicucci, G. Biasiol, and L. Sorba, Appl. Phys. Lett. **87**, 051105 (2005).

[6] R. Huber, A. A. Anappara, G. Günter, A. Sell, G. Biasiol, L. Sorba, A. Tredicucci, S. De Liberato, C. Ciuti, and A. Leitenstorfer, J. Phys.: Conf. Ser. **193**, 012060 (2009).

[7] C. Ciuti, G. Bastard, and I. Carusotto, Phys. Rev. B **72**, 115303 (2005).

[8] A. Auer and G. Burkard, Phys. Rev. B **85**, 235140 (2012).

[9] S. De Liberato and C. Ciuti, Phys. Rev. B **79**, 075317 (2009).

[10] R. Colombelli, C. Ciuti, Y. Chassagneux, and C. Sirtori, Semicond. Sci. Technol. **20**, 985 (2005).

[11] S. De Liberato, C. Ciuti, and C. C. Phillips, Phys. Rev. B **87**, 241304 (2013).

[12] Previous measurements of the sample (denoted NT3557) in 2003 by Dupont *et al.* [2] were limited by the angular resolution of the thermal source used. Intersubband cavity polariton linewidths reported there did not display the linewidth-narrowing effects and could only measure minimum ICP linewidths of 6.4 meV, compared to e.g. $\delta_{UPB} = 4.3$ meV measured here.

[13] D. M. Whittaker, P. Kinsler, T. A. Fisher, M. S. Skolnick, A. Armitage, A. M. Afshar, M. D. Sturge, and J. S. Roberts, Phys. Rev. Lett. **77**, 4792 (1996).

[14] C. Ell, J. Prineas, T. R. Nelson, S. Park, H. M. Gibbs, G. Khitrova, S. W. Koch, and R. Houdré, Phys. Rev. Lett. **80**, 4795 (1998).

[15] M. Załużny and C. Nalewajko, Phys. Rev. B **59**, 13043 (1999).

[16] Previous numerical simulations of the sample (Ref. [3], Structure $\mathcal{B}$) treated the ISBT absorption as purely a Lorentzian with a fixed δ_{ISBT}.

[17] Pochi Yeh, *Optical Waves in Layered Media* (Wiley, New York, 1988).

[18] E. R. Weber, R. K. Willardson, H. C. Liu, and F. Capasso, *Semiconductors and Semimetals: Intersubband Transitions in Quantum Wells: Physics and Device Applications I* (Academic Press, London, 2000).

[19] T. Unuma, M. Yoshita, T. Noda, H. Sakaki, and H. Akiyama, J. Appl. Phys. **93**, 1586 (2003).

[20] G. Beadie, W. S. Rabinovich, D. S. Katzer, and M. Goldenberg, Phys. Rev. B **55**, 9731 (1997).

[21] F. W. J. Olver, *NIST Handbook of Mathematical Functions* (Cambridge University Press, New York, 2010).